Surface chemical potential and current-density maps during annealing

M. V. Ramana Murty*
5530 Owensmouth Avenue, No. 213, Woodland Hills, California 91367, USA
(Received 20 January 2004; revised manuscript received 10 May 2004; published 24 September 2004)

A method is described to determine maps of surface chemical potential and current density on dynamic surfaces directly from discrete kinetic Monte Carlo simulations. It can be applied everywhere on the surface including the neighborhood of steps. The technique is used to investigate the decay of a bidirectional sinusoidal profile below the roughening temperature. For diffusion-limited kinetics driven by atom detachment and terrace diffusion, simulations indicate that the current density is proportional to the gradient of the chemical potential even with a cusp in the surface free energy.

DOI: 10.1103/PhysRevB.70.125424 PACS number(s): 68.35.Fx, 68.35.Ja

I. INTRODUCTION

The morphology of a material evolves continuously toward its equilibrium shape in the absence of external forces. This change is driven by a reduction in the total surface-free energy. The approach to equilibrium can be speeded up by annealing at high temperature. Surface diffusion is often the dominant mechanism responsible for the change in surface morphology.

An analytical description of the evolution of surface morphology during annealing was developed by Herring[1] and Mullins.[2] Mass flow is driven by variations in the chemical potential across the surface. The Herring-Mullins theory is readily applicable to amorphous materials. For crystalline materials below the roughening temperature T_R, cusps in the surface-free energy make it difficult to evaluate the chemical potential. Cusps correspond to low-index orientations (facets) of the material.

Several techniques have been proposed for describing the evolution of surface morphology of a crystalline material below T_R. These include several continuum methods[3–7] and step models.[8–12] For a given surface morphology, there are substantial differences in the magnitude of the chemical potential among these various methods. In addition, all these techniques use the standard irreversible thermodynamics relation between surface current and chemical potential. However, validity of this relation in the presence of a cusp in the surface-free energy has not been established.

In this paper, a method is described to calculate chemical potential and current density maps directly from kinetic Monte Carlo (KMC) simulations. For diffusion-limited kinetics on a rough surface below T_R, the simulations suggest that the current density is proportional to the gradient of the chemical potential on plateaus as well as sloped regions. These results support a continuum description of surface morphology evolution below T_R based on a rounded cusp.[3]

II. OBTAINING MICROSCOPIC PARAMETERS FROM MONTE CARLO SIMULATIONS

A rough surface morphology consists of steps separated by terraces. Relaxation of the surface occurs through the formation and migration of defects, such as adatoms and vacancies. At equilibrium, the adatom density is constant ($=n_{eq,a}$). Under nonequilibrium conditions, the adatom density varies across the surface to reflect the local arrangement of steps. The adatom chemical potential μ_a (in excess of its equilibrium value) at any point can be related to its density n_a through

$$\mu_a = k_B T \ln\left(\frac{n_a}{n_{eq,a}}\right). \tag{1}$$

Here, k_B is the Boltzmann constant and T is the temperature. Thus, a chemical potential map can be obtained by determining the adatom density at each point. However, the adatom density is extremely low in most situations. In practice, we evaluate the adatom density at a given site over a finite interval of time. Suppose a given site (i,j) is occupied by an adatom for an interval Δt_a over a period Δt. The adatom density is

$$n_a = \frac{\Delta t_a}{(\Delta t \cdot c_a)}. \tag{2}$$

Here, c_a is the adatom occupancy factor and represents the fraction of time that the site is available to an adatom. In a nearest-neighbor model on a square lattice, the site (i,j) is considered available[13] to an adatom when none of the four neighboring sites $(i-1,j)$, $(i+1,j)$, $(i,j-1)$, and $(i,j+1)$ are occupied, i.e., have height greater than or equal to site (i,j). An analogous definition applies to vacancies.

Surface current from site (i,j) to $(i+1,j)$ is determined from the number of hops between the two sites. In a given interval Δt, suppose p_+ and p_- represent the number of hops from $(i,j)\rightarrow(i+1,j)$ and $(i,j)\leftarrow(i+1,j)$, respectively. Then, the current at $(i,j)\rightarrow(i+1,j)$ is

$$j = \frac{p_+ - p_-}{\Delta t}. \tag{3}$$

Note that the current includes all atoms and not just adatoms.

KMC simulations are performed on a solid-on-solid model with a square lattice. The energy associated with an atom is $-n\varepsilon$, where n is the number of in-plane nearest

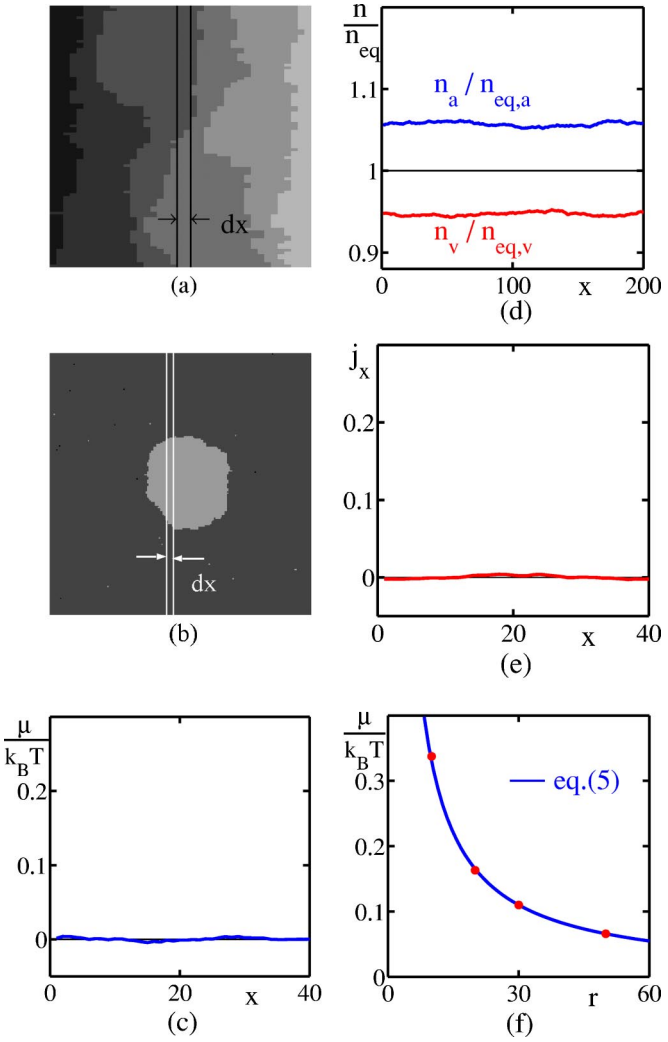

FIG. 1. (Color online) (a) Snapshot of a vicinal surface at temperature $T=0.4\ T_R$. The average terrace width is 8 lattice units. The stripe of width dx indicates the lattice sites over which the adatom and vacancy densities are averaged. (b) Snapshot of an island in equilibrium with adatoms and vacancies at $T=0.4\ T_R$. There are nominally 3600 atoms in the island. (c) Chemical potential on the vicinal surface as a function of position evaluated with $dx=1$. (d) The adatom and vacancy densities across the surface in equilibrium with the two-dimensional island, evaluated with stripe width $dx=1$. (e) Surface current on the vicinal surface evaluated with $dx=1$. (f) The variation of chemical potential with island size follows the Gibbs-Thompson expression, Eq. (5).

neighbors. Only nearest neighbor hops are allowed. The jump frequency f from site 1 with energy E_1 to site 2 with energy E_2 is

$$f = \nu \exp[-(E_2 - E_1 + \varepsilon_d)/k_B T], \quad E_1 < E_2$$
$$= \nu \exp(-\varepsilon_d/k_B T), \quad E_1 \geqslant E_2. \tag{4}$$

Here, ν is the attempt frequency. The activation barrier for terrace diffusion of adatoms (and vacancies) is ε_d. The formation energy of an adatom (and vacancy) is 2ε. Time t is measured in units of Monte Carlo steps (MCS) where $1\ \mathrm{MCS} = \nu^{-1} \exp(\varepsilon_d/k_B T)$. The roughening temperature is

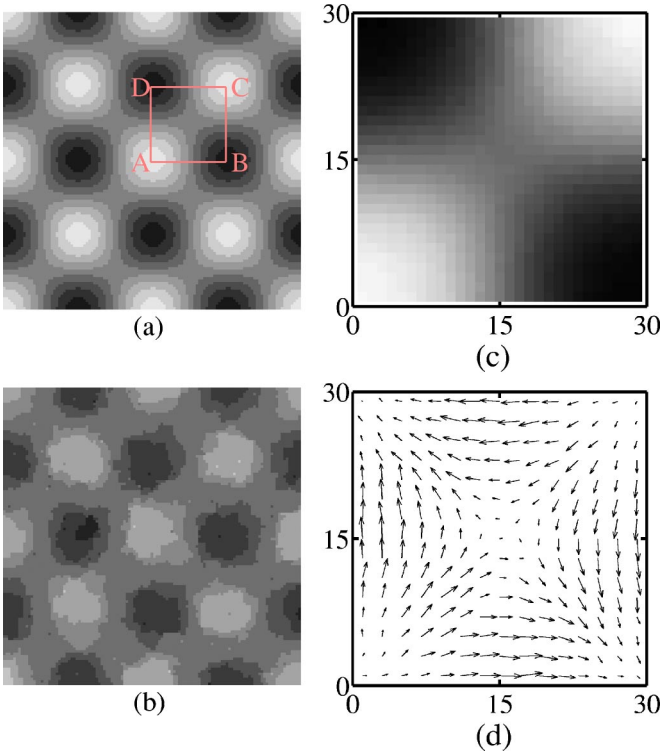

FIG. 2. (Color online) (a) The starting surface of a bidirectional sinusoidal profile with wavelength $L=60$. The simulations are performed on a 300×300 surface and a 120×120 section is shown here. In calculating the adatom and vacancy densities and the surface current, all regions equivalent to the square ABCD are averaged. (b) Snapshot of the $L=60$ surface at $\tau=0.93$. (c) Chemical potential map evaluated at $(\tau,\Delta\tau)=(0.93,0.19)$. (d) A vector map of the current density at $(\tau,\Delta\tau)=(0.93,0.19)$. The length of the arrows indicates the magnitude of current. Mass flow is directed from the peaks (points A and C) to the valleys (points B and D).

$T_R = 0.62\varepsilon/k_B$.[14] Appropriate periodic boundary conditions are applied in the transverse directions. There is no additional step-edge (Ehrlich-Schwoebel) barrier leading to diffusion-limited kinetics.

We first consider two simple geometries, a vicinal surface and a two-dimensional island in equilibrium with adatoms and vacancies. Figure 1(a) shows a snapshot of a vicinal surface with an average terrace width of 8 lattice units. The simulation was performed on a 40×2000 surface at $T=0.4\ T_R$ [a 40×100 section is shown in Fig. 1(a)]. The adatom chemical potential across the surface evaluated over $\Delta t = 2\times10^7$ and averaged over stripe width $dx=1$ (lattice unit) is shown in Fig. 1(c). As expected, $\mu_a = 0$ within statistical error. Likewise, Fig. 1(e) shows that the current density j_x vanishes across the surface. The equilibrium adatom and vacancy density $n_{eq,a} = n_{eq,v} = 3.17\times10^{-4}$ (per lattice site) is in agreement with the expected value $\exp(-2\varepsilon/k_B T) = 3.17\times10^{-4}$.

Figure 1(b) shows a snapshot of a two-dimensional island at $T=0.4\ T_R$. The use of periodic boundary conditions prevents evaporation of the island by allowing the adatom and vacancy density to build up to equilibrium values.[15] The simulation was performed on a 200×200 surface and there

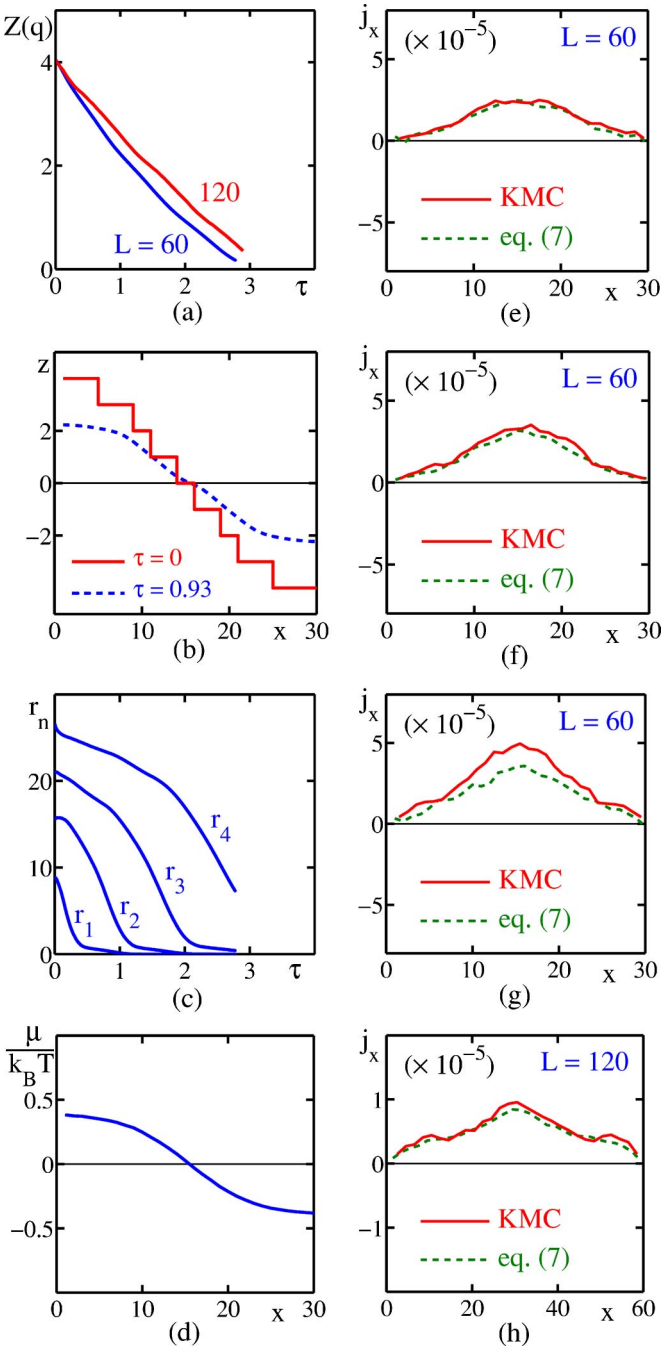

FIG. 3. (Color online) (a) Evolution of the Fourier amplitude $Z(\mathbf{q})$, $\mathbf{q}=(2\pi/L,2\pi/L)$, for bidirectional sinusoidal profiles with wavelengths $L=60$ and 120. (b) Average surface height along the line AB (see Fig. 2) at $\tau=0$ and 0.93 for $L=60$. (c) Variation of the island size as a function of reduced time τ. (d) Variation of $\mu/k_BT=(\mu_a-\mu_v)/k_BT$ along the line AB for $L=60$ at $(\tau,\Delta\tau)=(0.93,0.19)$. (e)–(h) Comparison of current density obtained directly from the KMC simulations with Eq. (7) at different times and for different wavelengths. The reduced time and interval $(\tau,\Delta\tau)$ are (e) (1.85, 0.19), (f) (0.93, 0.19), (g) (0.19, 0.19), and (h) (0.12, 0.35), respectively. The simulations for $L=60$ and $L=120$ were performed on 300×300 and 360×360 surfaces, respectively.

are nominally 3600 atoms in the island. Figure 1(d) shows the adatom and vacancy density in equilibrium with the island evaluated over $\Delta t=4\times10^8$ and $dx=1$.[16] Both are uniform across the surface within statistical error. The adatom density increases whereas the vacancy density decreases from its equilibrium value, in accordance with the Le Chatelier-Braun principle.[17] Since the free energy of formation of an adatom and a vacancy is the same in the KMC model, the magnitude of change is the same for both defects. Figure 1(f) shows the variation of $\mu/k_BT=(\mu_a-\mu_v)/k_BT$ as a function of the island size. We observe the expected Gibbs-Thomson relation

$$\mu=\frac{\alpha\Omega}{h}\frac{G_1}{r}. \tag{5}$$

Here, G_1 is the step-free energy per unit length, r is the island size, h is the step height, Ω is the atomic volume, and α is a geometry factor. Taking $r=\sqrt{N}/2$ where N is the nominal number of atoms in the island, $\alpha G_1=0.82\varepsilon$.[18] The Gibbs-Thomson relation has also been observed in previous Monte Carlo simulations.[15] Note that the Gibbs-Thomson phenomenon only expresses a relation between vapor pressure and interface free energy, and is not restricted to circular islands.

III. EVOLUTION OF BIDIRECTIONAL SINUSOIDAL PROFILE

We now consider the decay of a bidirectional sinusoidal profile below T_R. The starting surface $z(x,y)$ is a discretized form of

$$z(x,y)=z_0\cos\left(\frac{2\pi x}{L}\right)\cos\left(\frac{2\pi y}{L}\right). \tag{6}$$

Previous KMC simulations with this model have shown that in the limit of long wavelength, the amplitude decays linearly with time with t/L^3 scaling.[3,19]

Snapshots of the surface during the decay of a bidirectional sinusoidal profile with $z_0=4$ and $L=60$ are shown in panels (a) and (b) of Fig. 2 at scaled time $\tau=t/L^3=0$ and 1.85, respectively. The simulations were performed on a 300×300 surface at $T=0.54\ T_R$. Chemical potential and current density are evaluated by averaging over all regions equivalent to the square ABCD indicated in Fig. 2(a). The chemical potential $\mu=\mu_a-\mu_v$ map evaluated at $\tau=0.93$ and $\Delta\tau=\Delta t/L^3=0.19$ is shown in Fig. 2(c). The chemical potential is highest at the peaks A and C and lowest at valleys B and D. A vector map of the current density is shown in Fig. 2(d). The length of the arrows indicates the magnitude of the current. Mass flow is directed from the peaks A and C toward the valleys B and D. Both the chemical potential and current density were obtained by averaging over 50 simulations.

The decay of the Fourier amplitude $Z(\mathbf{q})$, $\mathbf{q}=(2\pi/L,2\pi/L)$, with time is shown in Fig. 3(a) for two different wavelengths $L=60$ and $L=120$. While a linear decay with time is observed for $L=120$, a faster-than-linear decay is observed at short times for $L=60$. The average surface profile along line AB [see Fig. 2(a)] is shown in Fig. 3(b) for $L=60$ at $\tau=0$ and 0.93. A plateau is observed near the peak

(and valley) at $\tau=0.93$ and is due to the lower free energy of the facet compared to sloped regions. The evolution of the *average* size of an island with time is shown in Fig. 3(c). The island size $r_n=\sqrt{N_n}/2$, where N_n is the number of atoms in layer n. The chemical potential along the line AB evaluated at $(\tau,\Delta\tau)=(0.93,0.19)$ is shown in Fig. 3(d). The chemical potential varies everywhere including the plateau.

In continuum theory, one uses the irreversible thermodynamics relation between current density and the chemcial potential.[1,2] With mass flow driven by adatoms and vacancies, the surface current is given by

$$\mathbf{j}=\frac{D_v n_{eq,v}}{k_B T}\nabla\mu_v-\frac{D_a n_{eq,a}}{k_B T}\nabla\mu_a. \tag{7}$$

The adatom diffusion coefficient $D_a=[\nu a^2\exp(-\varepsilon_d/k_B T)]/4$ where a is the lateral lattice constant. A similar expression holds for D_v.

We now compare the surface current density calculated using Eq. (7) with that obtained directly from the KMC simulations. The chemical potentials μ_a and μ_v in Eq. (7) are determined from the KMC simulations. Panels (e)–(g) of Fig. 3 show the comparison at three different times for wavelength $L=60$. The current density is evaluated along the line AB [see Fig. 2(a)]. The agreement is good at all locations at late times $\tau=1.85$ and 0.93. Even at $\tau=0.19$, the agreement is better in the flat regions compared to regions of high slope. With $L=60$ and $z_0=4$, the starting surface has regions where the step separation is only one lattice unit [see Fig. 3(b)]. In such situations, atoms can move from one terrace to another without diffusion across the terrace. This current is not captured by Eq. (7). As the amplitude decreases, the step separation increases and decay proceeds more by atom detachment from steps and diffusion on the terrace. If we start with a longer wavelength $L=120$ and the same starting amplitude $z_0=4$, decay largely occurs by atom detachment and diffusion. Good agreement with Eq. (7) is then found even at short times as shown in Fig. 3(h). These results indicate that the irreversible thermodynamics relation between current density and chemical potential is valid even in the presence of a cusp in the surface free energy.

IV. DISCUSSION

The results of the KMC simulations support a continuum theory of surface relaxation based on a rounded cusp.[3] In this approach, the first step involves evaluating the chemical potential for a given surface morphology. The chemical potential is evaluated at each location assuming that it is in local equilibrium. Since the surface-free energy with the rounded cusp produces the correct equilibrium shape (in the limit of a small-rounded region), it also yields the correct chemical potential on the nonequilibrium surface. In particular, the continuum theory predicts a varying chemical potential on the plateaus as well as sloped regions of the surface.[3] The simulations above indeed show that the chemical potential varies over the plateaus. On the other hand, step models predict a constant chemical potential in flat regions,[8–11] which is inconsistent with the KMC results. Specifically, the chemical potential for the average surface $\mu(\langle z(r)\rangle)$ is different from the one evaluated using the average position of steps $\mu(z\langle r_n\rangle)$[3]. Once the chemical potential is known, mass flow is given by Eq. (7) in the continuum theory. The KMC simulations indicate *quantitative* agreement with this expression (for small slopes). The final step in the continuum theory is mass conservation, a feature also present in the KMC model.

V. CONCLUSION

Chemical potential and current density maps on nonequilibrium surfaces have been determined directly from kinetic Monte Carlo simulations. On a bidirectional sinusoidal profile below T_R, chemical potential is found to vary on both the plateaus and sloped regions of the surface. For diffusion-limited kinetics, the simulations indicate that the irreversible thermodynamics relation between current density and chemical potential is valid even when a low-index orientation forms part of the surface. These results support a continuum theory of surface morphology evolution based on a rounded cusp.[3]

M.V.R.M would like to thank J. Villain for a useful discussion on the various issues regarding diffusion on crystalline surfaces.

*Electronic address: mvrmurty@e2oinc.com

[1] C. Herring, *Structure and Properties of Solid Surfaces*, edited by R. Gomer and C. S. Smith (University of Chicago Press, Chicago, 1952), p. 1.

[2] W. W. Mullins, *Metal Surfaces: Structure, Energetics and Kinetics*, edited by N. A. Gjostein and W. D. Robertson (ASM, Metals Park, OH, 1963), p. 99.

[3] M. V. R. Murty, Phys. Rev. B **62**, 17004 (2000).

[4] H. Spohn, J. Phys. I **3**, 69 (1993).

[5] J. Hager and H. Spohn, Surf. Sci. **324**, 365 (1995).

[6] N. Israeli and D. Kandel, Phys. Rev. Lett. **88**, 116103 (2002).

[7] V. B. Shenoy, A. Ramasubramaniam, and L. B. Freund, Surf. Sci. **529**, 365 (2003).

[8] A. Rettori and J. Villain, J. Phys. (Paris) **49**, 257 (1988).

[9] M. Ozdemir and A. Zangwill, Phys. Rev. B **42**, 5013 (1990).

[10] M. Uwaha, J. Phys. Soc. Jpn. **57**, 1681 (1988).

[11] N. Israeli and D. Kandel, Phys. Rev. Lett. **80**, 3300 (1998).

[12] S. Tanaka, N. C. Bartelt, C. C. Umbach, R. M. Tromp, and J. M. Blakely, Phys. Rev. Lett. **78**, 3342 (1997).

[13] With this definition the sites adjacent to an adatom are considered unavailable. However, they are available to the adatom itself. The error caused thereby is small because the adatom densities considered here are low.

[14] W. J. Shugard, J. D. Weeks, and G. H. Gilmer, Phys. Rev. Lett. **41**, 1399 (1978).

[15] B. Krishnamachari, J. McLean, B. Cooper, and J. Sethna, Phys.

Rev. B **54**, 8899 (1996).

[16] The adatom and vacancy density is identical at every site. While averaging is carried out for a rectangular group of cells in Fig. 1(d), grouping into circular shells with varying distance from the center will yield the same result.

[17] H. B. Callen, *Thermodynamics and an Introduction to Thermostatistics*, 2nd ed. (Wiley, New York, 1985), Chap. 8.

[18] The factor α depends on the equilibrium shape of the island and takes the values 1 and $\sqrt{\pi}/2$ for a square (shape at $T=0$ K) and a circle (shape at high temperature), respectively.

[19] M. V. R. Murty and B. H. Cooper, Phys. Rev. B **54**, 10377 (1996).